Applied Catalysis A: General 470 (2014) 327–335

Contents lists available at ScienceDirect

Applied Catalysis A: General

journal homepage: www.elsevier.com/locate/apcata

Photocatalytic conversion of methane into methanol: Performance of silver impregnated WO_3

A. Hameed[a,b], Iqbal M.I. Ismail[a,d], M. Aslam[a], M.A. Gondal[c,*]

[a] Centre of Excellence in Environmental Studies (CEES), King Abdulaziz University, Jeddah 21589, Saudi Arabia
[b] National Centre for Physics, Quaid-e-Azam University, Islamabad 44000, Pakistan
[c] Department of Physics, King Fahd University of Petroleum and Minerals, Dhahran 31261, Saudi Arabia
[d] Department of Chemistry, Faculty of Science, King Abdulaziz University, PO Box 80203, Jeddah 21589, Saudi Arabia

ARTICLE INFO

Article history:
Received 21 May 2013
Received in revised form 22 October 2013
Accepted 25 October 2013
Available online 4 November 2013

Keywords:
Photocatalysis
Methane conversion
Methanol
Silver impregnated WO_3

ABSTRACT

A detailed investigation of photocatalytic conversion of methane into methanol, over Ag^+ impregnated WO_3, is reported. The intense monochromatic light source, 355 nm laser photons exposure, facilitated the study of complex processes in short span of time. The characterization techniques, XRD and XPS, confirmed that Ag^+ ions share surface oxygen with WO_3 to give Ag_2O, which enhanced the absorption of photons, lifetime of excited states. The study encircled all the processes that occur on the surface of the catalysts as well as in the bulk that included water splitting, methanol formation as a result of methane conversion and degradation of methanol immediately after its formation. The measurement of evolved H_2 and O_2 in the gaseous phase and methanol in the liquid phase revealed that the methanol, instantly after its formation, competes with water molecules for the photogenerated holes and decomposes. Efforts have been made to correlate all the processes involved and to estimate the plausible mechanism for *in-situ* methane conversion and methanol degradation.

1. Introduction

Photocatalysis, owing to its mineralization feature, is widely studied for water purification that includes water decontamination and disinfection [1–5]. Although least explored, another avenue of photocatalysis is the conversion of chemically inert molecules such as methane into useful oxygenates. Methane, being naturally abundant, is the simplest hydrocarbon having low C:H ratio and high calorific value with a wide range of uses as fuel in fertilizer, petrochemical, automobile industry. Methane being the part of greenhouse gases also contributes to global warming therefore it is desirable to convert methane into liquid transportable fuels such as methanol, as it retains most of methane energy, for safe transportation and clean environment using economically viable and easily accessible resources. The conventional technologies in use to convert methane into alternative fuels, such as initial conversion of methane into syngas (mixture of H_2 and CO) followed by high temperature catalytic conversion of syngas to methanol, are not cost effective [6–10].

The use of light and water to convert methane into methanol is an attractive option. Photochemical conversion of methane into methanol via direct photolysis approach i.e. the free radical interaction of photo-generated hydroxyl radicals with the methane molecules is reported in the literature [11–14]. However the requirement of 185 nm photons for the generation of hydroxyl radicals, poor yield and selectivity of the desired product, methanol, are the limitations associated with direct photolysis. Heterogeneous photocatalysis is a promising approach in this regard, as it deals with the formation of cascade of highly energetic hydroxyl radicals at the surface of semiconductor photocatalyst in the aqueous medium under illumination. Prior studies [15–18] reported that methane can be converted to methanol and other useful oxygenates in the presence of lanthanum doped WO_3, in the presence of water vapors at 90 °C under illumination. A number of researchers using a variety of catalyst other than WO_3 and varying experimental conditions [19–25] studies the photocatalytic oxidation of methane. In our previous studies [26,27], we reported the conversion of methane into methanol under visible (514 nm) over WO_3 as well as ultraviolet (355 nm) laser exposure over WO_3, TiO_2, NiO and Fe_2O_3. The present study is a step ahead in the same direction as it was designed after the careful analysis of the results of previous studies. To achieve the maximum charge separation and enhanced generation of hydroxyl radicals, the surface of WO_3 was modified by impregnating Ag^+ ions. It has been attempted to explore all the processes occurring simultaneously under illumination that includes water splitting, interaction of photo-generated hydroxyl radicals ($OH^•$) with methane to form methanol, interaction of methanol after its formation with hydroxyl radicals and the possible role of

* Corresponding author.
E-mail address: magondal@kfupm.edu.sa (M.A. Gondal).

0926-860X/$ – see front matter © 2013 Elsevier B.V. All rights reserved.
http://dx.doi.org/10.1016/j.apcata.2013.10.045

methanol as sacrificial agent. The estimation of plausible mechanism is based on:

- H_2 and O_2 measurement during water splitting process.
- H_2 and methanol measurements during methane conversion process.
- H_2 and methanol measurements during methanol degradation studies.

2. Experimental

2.1. Synthesis of Ag^+ impregnated WO_3

Ag^+ impregnated WO_3, containing different proportions of Ag^+ (w/w) with respect to WO_3, were synthesized by wet impregnation technique [28]. In the typical synthesis, the required proportions of Ag^+ ions (0.1%, 1.0%, 5% and 10%) were prepared by dissolving $AgNO_3$ (99.9%) in deionized water and mixed with the appropriate quantity of WO_3 derived from H_2WO_4 as detailed elsewhere [26]. The slurry containing silver ions and WO_3 was aged overnight under stirring and the excess water was dried at 100 °C. The nitrates were decomposed by heating at 300 °C with vigorous stirring. The dried powders were calcined in temperature-controlled furnace at 400 °C for 3 h by maintaining the heating rate at 10 °C/min.

2.2. Characterization of Ag^+ impregnated WO_3

The UV–Visible spectra of the stable aqueous suspension of impregnated powders were acquired by using SHIMADZU 1800 UV–Visible spectrophotometer using water as reference and a slit width of 1.0 nm. The measurements were repeated to examine the accuracy and reproducibility of the process. A Scintag XDS 2000 diffractometer, equipped with a Cu $K\alpha$ radiation source, was used to record the XRD patterns of the synthesized powders in the range of 0° to 90°. The obtained patterns were matched with standard JCPDS cards for identifying the existing phases. The crystallite sizes of the contributing phases were calculated by applying Scherer's equation on the FWHM values of the intense reflections. The FESEM (JEOL JSM 6490-A) was used to examine the morphology of synthesized powders. The XPS profiles of Ag^+ impregnated powders were acquired by a wide survey scan using X-ray Photoelectron Spectrometer (PHI 5000 VersaProbe II, ULVAC-PHI Inc.). The binding energy was varied between 0 eV to 1100 eV. The oxidation states of the surface bonded impregnated Ag^+ ions were evaluated on the basis of the splitting arises due to spin-orbit coupling.

2.3. Experimental details for photocatalytic studies

The photocatalytic studies were performed in a self-fabricated photocatalytic reactor [29]. The earlier studies [26,27,29], revealed that the variations in experimental parameters such as laser energy, laser beam diameter, stirring rate and amount of catalyst affects the products yield significantly during laser based photocatalytic experiments. Keeping in view the preceding observations, beam diameter and stirring rate were kept constant at 8 mm and 1000 rpm respectively while the catalyst loading and laser beam energy were carefully optimized for maximum yield of dissolved oxygen (Hanna Model, HI 9143) in water splitting experiments. The detailed experimental setup and procedure for the optimization of amount of catalyst and laser beam energy is described elsewhere [26,27,29].

All the photocatalytic studies were performed as batch process. Photocatalytic splitting of water over Ag^+ impregnated WO_3 was studied by suspending 300 mg of photocatalyst in 70 cm^3 of distilled water. An inert atmosphere was produced by purging argon (Ar) gas at a high flow rate for complete exclusion of dissolved oxygen. The progress of argon purging was monitored by analyzing the gas sample from the dead volume of reactor. The suspension containing Ag^+ impregnated WO_3 photocatalyst, water and argon gas was exposed to 100 mJ, 355 nm laser beam for 90 mins. The progress of the reaction was monitored by drawing 100 μL samples by a gas tight syringe at regular intervals. Calibrated gas chromatograph (SHIMADZU, GC-17A), equipped with thermal conductivity detector (TCD) and a 30 m molecular sieve 5A "PLOT" column was used to analyze H_2 and O_2 evolved during photocatalytic water splitting process. High purity (99.999%) argon (Ar) gas was used as carrier.

For methane conversion experiments, the same procedure as detailed in water splitting experiments was adopted. Additionally, methane was supplemented at a flow rate of 100 cm^3/min for a period of 15 mins after expelling oxygen by argon purging. Hydrogen (H_2) in the gas phase and methanol in the liquid phase was monitored for evaluating the progress of reaction. 10 μL liquid samples were analyzed by using a gas chromatograph (GC 6890, Agilent Technologies) equipped with an FID detector and 2 m Chromosorb-101 packed column in split less mode. Helium (He) gas was used as carrier.

Photocatalytic methanol degradation experiments were performed by adding 10 μL of methanol in argon purged catalyst suspension. The progress of the reaction was estimated by measuring H_2 from the dead volume of the cell and methanol from the suspension at regular intervals by using the gas chromatographs detailed in the previous experiments. The reproducibility of all the processes was checked by repeating the experiments at the regular intervals while the reproducibility of the analysis was estimated by running the standards time to time. The uncertainty in the measurement of yield of various products was less than 3%, which was acceptable for the purpose of present studies. All the reactions were carried out at room temperature (23 °C).

3. Results and discussion

3.1. Absorption spectra and band gap determination

The absorption spectra of pure and Ag^+ impregnated WO_3 were recorded in the aqueous environment from 200 nm to 1000 nm. An enhanced absorption in the visible region was observed in the visible region with the increasing Ag^+ loading. A red shift in the absorption maximum compared to that of 316.5 nm for pure WO_3 was observed for all catalysts. The absorption spectra of the synthesized catalysts are presented in Fig. 1. In pure WO_3, the major transitions are the transfer of electrons from the oxygen 2p orbitals (valence band) to 4f *orbitals* (conduction band) of W^{6+} or W^{5+} states. The contribution of f–f transitions cannot be neglected in this regard. The insertion of Ag^+ at the surface induces the low laying d-*orbitals* at the surface. The transitions of valence band electrons (O 2p) to the low laying Ag 3d *orbitals* enhance the absorption of photons in the visible region. Additionally the transitions between Ag d–d states are an additive factor.

The band gaps of the synthesized powders were estimated by fitting the absorption data as mentioned in the literature [30–32].

$$\alpha h\nu = B(E_g - h\nu)^{1/2}$$

Absorption coefficient α based on absorbance (A) and path length (l) is given as:

$$\alpha = \frac{1}{l}\frac{A}{\log e}$$

The bandgap of the synthesized materials were evaluated by extrapolating the plots of $h\nu$ versus $(\alpha h\nu)^2$ for pure and Ag^+

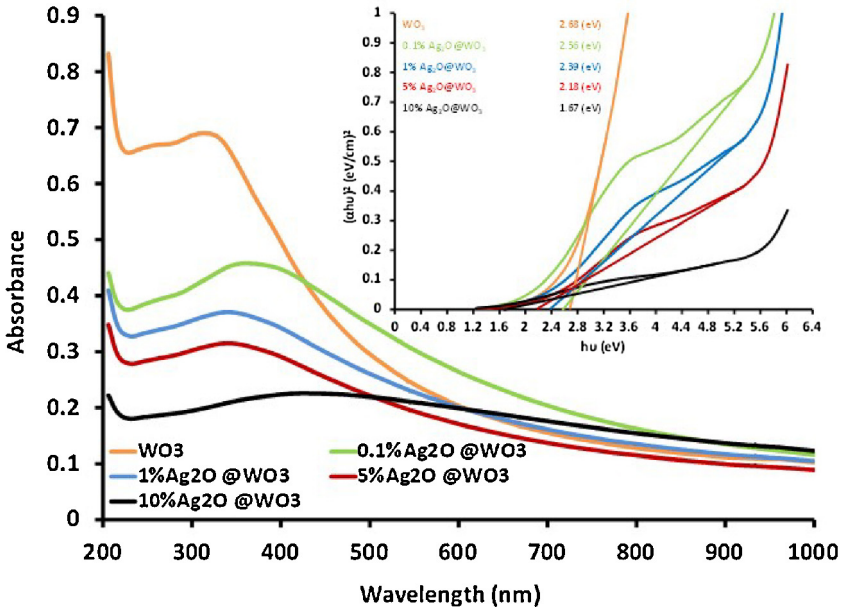

Fig. 1. Aqueous phase absorption spectra of pure and Ag^+ impregnated WO_3. The onset shows the graphical evaluation of bandgaps.

impregnated WO_3 photocatalysts. The increasing loading of Ag^+ ions shifted the bandgaps in the longer wavelength region. The graphical representation of bandgap evaluation and the evaluated bandgaps are presented in the onset of Fig. 1.

3.2. X-ray Photoelectron spectroscopy

The XPS spectra of pure and Ag^+ impregnated WO_3, obtained by wide survey scan between 0 eV and 1100 eV is shown in Fig. 2a. From the survey scan of Ag^+ impregnated WO_3, peaks of O 1s, W 4f and Ag 3d are clearly observed in all the spectra. The careful comparison of XPS patterns of pure and Ag^+ impregnated WO_3 samples revealed the asymmetric nature of the peaks for the impregnated samples while no peak was observed for pure WO_3. The asymmetry of Ag 3d peaks (Fig. 2b) clearly indicates the existence of more than one oxidation state of Ag at the surface, which may be represented as AgO_x. The broadening and deformation of Ag 3d peaks increases

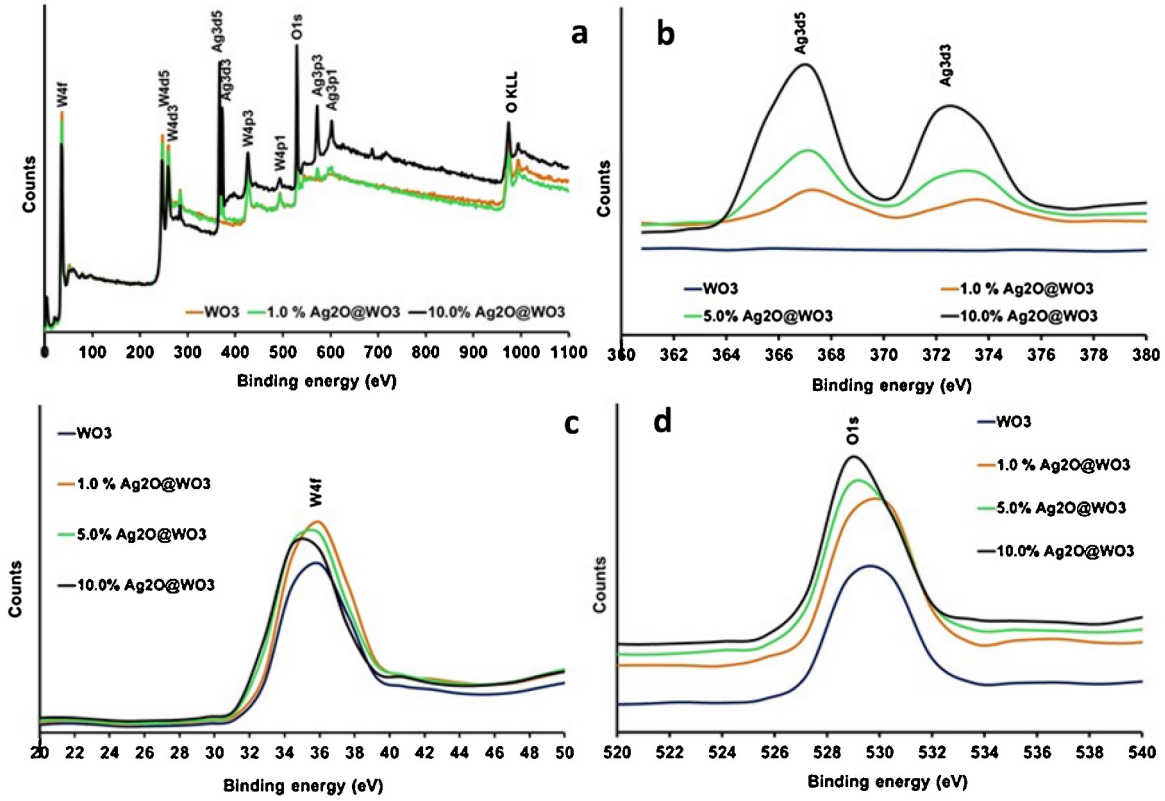

Fig. 2. XPS profile of Ag impregnated WO_3: (a) Comparison of the survey scan of pure, 1% and 10% Ag^+ impregnated WO_3. (b) Comparison of Ag 3d split levels in 1%, 5% and 10% Ag^+ impregnated WO_3. (c) Comparison of W 4f levels in pure, 1%, 5% and 10% Ag^+ impregnated WO_3. (d) Comparison of O 1s profiles of pure, 1%, 5% and 10% Ag^+ impregnated WO_3.

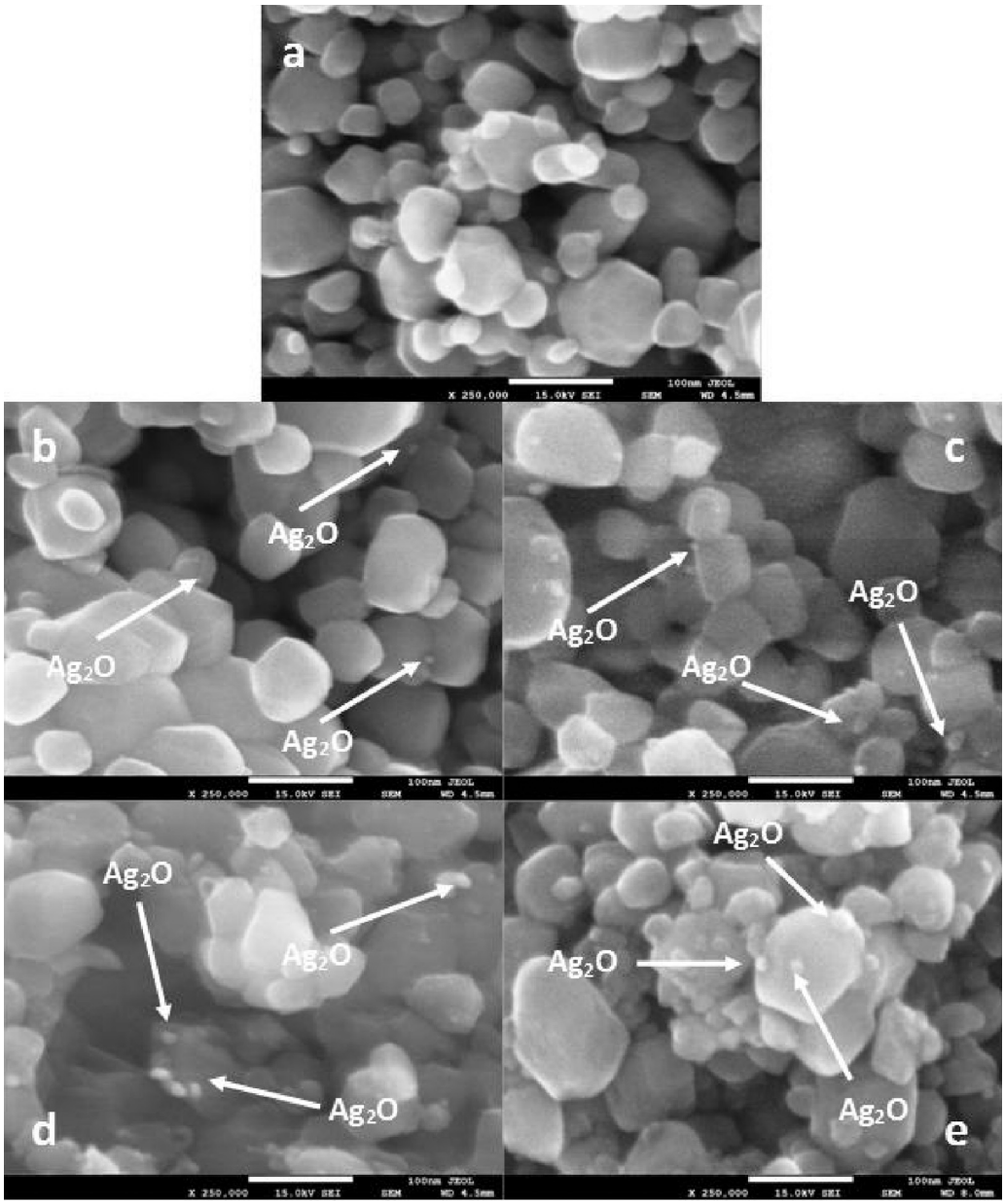

Fig. 3. FE–SEM high resolution images (x 250,000) of pure and Ag^+ impregnated WO_3.

with the increase in Ag content ensuring the presence of mixed oxidation states at the surface. The Ag $3d_{5/2}$ peak at 367.4 eV compared to that for metallic Ag at 368.2 eV [33,34] confirming the existence of impregnated Ag^+ as surface Ag_2O rather than elemental silver for 0.1% and 1% impregnated samples. Also the binding energy of Ag $3d_{5/2}$ and the difference between the two levels i.e. 6.0 eV confirmed the presence of Ag as Ag^+ at the surface of WO_3 and the chemical form was predicted as Ag_2O for low concentration of Ag^+. The obtained values were in agreement with the literature values of 367.3–367.6 for Ag_2O [35]. For 5% and 10% impregnated samples, a shift of 0.4 eV in the observed E_b values of split Ag $3d_{5/2}$ indicates the existence of AgO_x, at the surface, originated by sharing the surface oxygen of WO_3 rather than existing as the free entity [36]. The chemically different nature of the binding sites leads to the shifting in the binding energy of the split levels compared to that of Ag_2O literature values [35]. For pure WO_3, due to existence of W^{6+} and W^{5+} states, the broad asymmetric peak of the W 4f core levels (Fig. 2c) corresponds to unresolved W $4f_{7/2}$ and W $4d_{5/2}$ states. The curve fitting of asymmetric peak revealed a pair of peaks at 34.4 and 36.1 eV that shows the dominance of W^{6+} oxidation state in the mixture of W^{6+} and W^{5+} states [37–41]. The peak broadening and shifting towards lower binding energy is attributed to the increasing Ag^+ loading at the surface. For pure WO_3, a broad asymmetric O 1s peak was observed. The binding energy of 529.8 eV coincides with O 1s binding energy (Fig. 2d) assigned to the oxygen in WO_x [42] and a minor component at 531.8 eV representing surface O–H groups was observed. The presence of a number of surface entities such as W–O–W, $W–O^-$ and WO_2, characteristic of non-stoichiometric monoclinic WO_3, are responsible for asymmetric nature of O 1s peak [43].

3.3. FE–SEM analysis

Field Emission Scanning Electron Microscope (FESEM) examined the morphology and size of the samples. The high-resolution FESEM images of pure and Ag impregnated WO_3, as presented in Fig. 3, where the surface Ag_2O particles can be identified and their number increases with the increase in surface density of Ag^+. It can

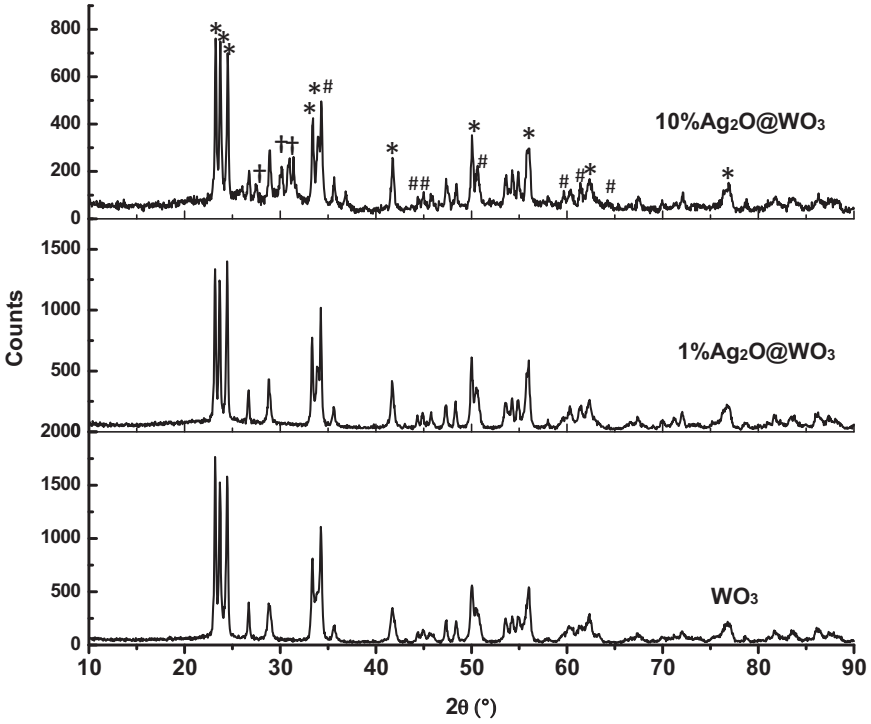

Fig. 4. Comparison of XRD patterens of pure 1% and 10% Ag^+ impregnated WO_3. The symbols *, # and † indcates the reflections arising from monoclinic WO_3, Ag_2O and Ag_2WO_4.

also be observed that the nanoparticles are quasi-spherical having diameter within the range of 20–40 nm. The Ag_2O particles reside at the surface of WO_3 without significantly affecting the morphology of base WO_3.

3.4. XRD- analysis

A comparison of XRD patterns of pure WO_3, 1%, and 10% Ag^+ impregnated WO_3 are presented in Fig. 4, where it can be observed that the reflections arising from WO_3 dominate in all the XRD patterns however the intensity of main reflections decreases with increasing concentration of Ag^+. The intense reflections at 2θ values of 23.14, 23.66, 24.45, 33.35, 34.25, 41.70 and 44.9, in all the patterns were matched with monoclinic WO_3 (JCPDS-43-1035), while the low intensity reflections entrapped in high intensity reflections at 34.22, 44.35, 46.23, 52.10 and 59.86 were matched with hexagonal Ag_2O (JCPDS-42-0874). Although other Ag species such as nano crystalline Ag, AgO and Ag_3O_4 were also identified but the reflections arising from these species were of very low intensity. For 10% Ag^+ impregnated sample, the reflections of moderate intensity at 2θ values of 25–35° were also observed. These reflections were matched with Ag_2WO_4 (JCPDS-32-1029). The formation of surface $Ag_2O{\cdot}WO_3$ is expected with the increasing Ag^+ contents on the surface. No significant change in the crystallite size of WO_3 was observed with increasing concentration of Ag^+. The average crystal sizes of pure and Ag^+ impregnated WO_3 calculated by applying Scherrer's equation on the most intense reflections were 43.7 nm, 44.1 nm, 44.9 nm, 45.6 nm and 44.2 nm for pure, 0.1%, 1%, 5% and 10% Ag^+ impregnated WO_3, respectively.

3.5. Photocatalytic studies

3.5.1. Photocatalytic splitting of water

The splitting of water into its components is an uphill process and requires ~235 kJ energy or photons of energy ≤6.7 eV corresponding to 185 nm. For a photocatalyst to cleave water i.e. the formation of hydroxyl radicals and generation of hydrogen ions, the valence band edge of the catalyst should be positive than +1.23 V. With the possibility of a number of side reactions that can occur at the surface of the catalyst and in bulk, photocatalytic splitting of water is a very complex reaction. In aqueous medium, the processes that are initiated with the absorption of photons by the photocatalyst are presented in Scheme 1.

$$WO_3 + h\upsilon \xrightarrow{E \geq Eg} h^+ + e^-$$

$$H_2O + h^+ \rightarrow OH^\bullet + H^+$$

$$OH^\bullet + OH^\bullet \rightarrow H_2O + {}^1\!/\!_2 O_2$$

In our previous communication [29], we explained the plausible reasons for the generation of non-stoichiometric H_2 and O_2 formation over pure WO_3 even in the presence of non-favorable conduction band edge i.e. (+0.4 V). The photon-generated defects were identified as trap and transfer sites for electrons to H^+ ions. Possibly, due to the inadequate loading of Ag^+, for 0.1% Ag^+ impregnated WO_3, no significant change in the photocatalytic activity was noticed. For 1% Ag^+ loading, as presented in Fig. 5(a), an increase in the H_2 yield was observed that is mainly due to the formation of surface traps induced by Ag^+ surface impregnation. These defects serve as trap and transfer centers for photogenerated electrons essential for H_2 generation. The possible mechanism of electron transfer from oxygen 2p orbitals (LUMO) is initially transferred to W 4f orbitals (HOMO) and then to the low laying d-*orbital* of surface

$$WO_3 + h\upsilon \xrightarrow{E \geq E_g} h^+ + e^-$$

$$H_2O + h^+ \rightarrow OH^\bullet + H^+$$

$$OH^\bullet + OH^\bullet \rightarrow H_2O + {}^1\!/\!_2 O_2$$

Scheme 1.

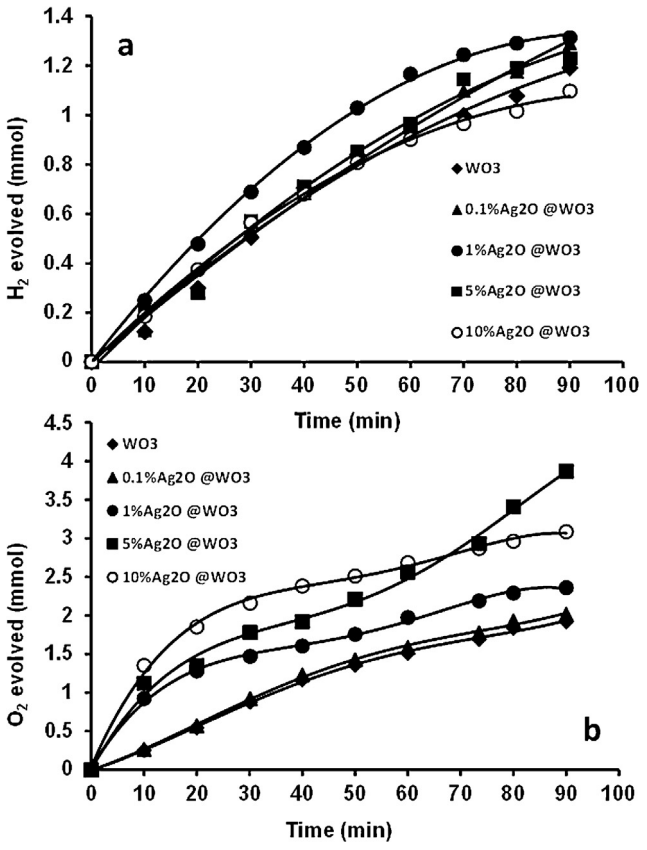

Fig. 5. (a) Comparison of H_2 production over pure and Ag^+ impregnated WO_3 photocatalysts under 100 mJ, 355 nm laser exposure for a period of 90 mins at 23 °C with a catalyst loading of 300 mg/70 cm^3. (b) Comparison of O_2 generation in water splitting process over pure and Ag^+ impregnated WO_3 photocatalysts under 100 mJ, 355 nm laser exposure at ambient (23 °C) temperature. The catalyst suspension (300 mg/70 cm^3) was purged with Argon gas for complete removal in the dark.

Ag^+ is presented in Fig. 6. The further increase in Ag^+ surface loading, as in case of 5% and 10% Ag^+ loading, suppressed the charge trap and transfer of electrons, which caused a substantial decrease in H_2. The direct absorption of photons by the silver entities and the non-suitability of band edges of surface Ag_2O for promoting H_2 formation are the major factor in this regard. However, as presented in Fig. 5(b), an increasing trend for O_2 generation was observed for 5% and 10% Ag^+ loading suggesting the suppression of photogenerated $e^- - h^+$ recombination with increased water oxidation i.e. increased yield of $OH^\bullet$ radicals and H^+ ions. The valence band edge positions of both Ag_2O (+1.39 V) and WO_3 (+3.1 V) [44] allows the migration of holes (h^+) generated by photon-induced

$$Ag_2O + h\nu \rightarrow 2Ag^+(sol) + \frac{1}{2}O_2^-(surface)$$

$$Ag^+(+0.8V) + e_{cb}^-(+0.7V) \rightarrow Ag^\circ$$

Scheme 2.

electronic excitation, from the valence band of WO_3 to the valence band of Ag_2O, thus enhancing the lifetime of excited states. On the other hand, the relocation of photogenerated electrons produced by the direct absorption of photons by Ag_2O to the conduction band of WO_3 is also energetically favored process. The possible mechanisms of hole (h^+) transfer and relocation of photogenerated electrons are presented in Fig. 7(a) and Fig. 7(b), respectively. The significant decrease in H_2 generation (Fig. 5 (a)) and initial increase followed by the decrease in O_2 formation with time (Fig. 5(b)), for 10% surface Ag^+, indicates that AgO_x species (mainly Ag_2O) absorbs the major portion of the incident photons. A significant red shift in λ_{max} in the absorption spectra (Fig. 1) supports the same finding. The observed deposition of metallic Ag° at the inner surface of the photocatalytic reactor indicated the depletion of silver contents on the surface of 10% impregnated photocatalyst. The enhancement of photocatalytic activity by surface plasmon resonance phenomenon is reported for metallic Ag, and Au nanoparticles loaded photocatalysts [39]; therefore, for Ag^+ impregnated WO_3, the possible contribution of surface plasmon resonance in enhancing the photocatalytic activity cannot be ignored. However, in this particular case, the binding of Ag^+ with the surface oxygen (in the form of Ag_2O) limits the role of surface plasmon resonance that requires metallic nanoparticles with free charges. Additionally, the intimate contact of plasmon resonance generating metallic nanoparticles with the host photocatalyst, for the injection of charge carriers, is essential as the plasmonic charge carriers, due to energy considerations are unable to generate oxidation or reduction reactions independently [45]. The proposed mechanism for the release of Ag^+ ions from the surface of WO_3 to the bulk and further reduction by the conduction band electrons to metallic silver (Ag°) is elaborated in Scheme 2.

$$Ag_2O + h\nu \rightarrow 2Ag^+(sol) + \tfrac{1}{2}O_2^-(surface)$$

$$Ag^+(+0.8V) + e_{cb}^-(+0.7\,V) \rightarrow Ag^\circ$$

3.5.2. Photocatalytic conversion of methane

Methane (CH_4) with completely engaged electronic arrangement is a chemically inert molecule. It lacks both adsorption at the surface of the photocatalyst and electron donating abilities to the photogenerated holes that suggests its conversion in the bulk rather than at the surface of the photocatalyst and necessitates the

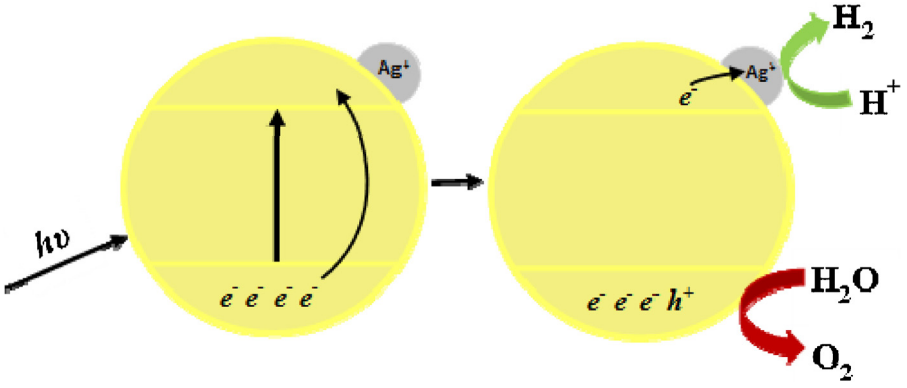

Fig. 6. The possible mechanism of electron capture by surface Ag^+ entities in impregnated WO_3 under illumination.

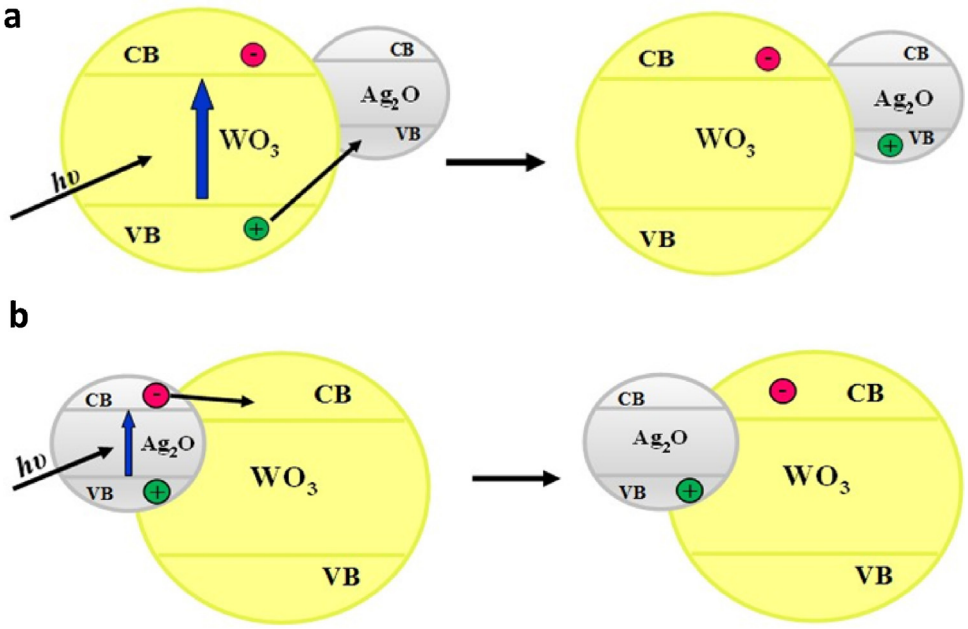

Fig. 7. Mechanism of e^-–h^+ pair recombination inhibition. (a) When the photons are absorbed by WO_3, the photogenerated holes (h^+) are transferred from to the valence band of WO_3 to the valance band of surface Ag_2O in energetically allowed transition. (b) When the photons are absorbed by surface Ag_2O, the photogenerated electrons (e^-) from the conduction band of Ag2O are transferred to the conduction band of WO_3.

increased generation of hydroxyl radicals through water oxidation. Scheme 3 accounts for all the possible reactions that occur in the bulk.

$CH_4 + OH^\bullet \rightarrow CH_3OH + H^\bullet$

$CH_3OH + OH^\bullet \rightarrow CH_2OH \rightarrow CO_2 + H_2O$

$H^\bullet + H^\bullet \rightarrow H_2$

$OH^\bullet + OH^\bullet \rightarrow H_2O + {}^1\!/\!_2 O_2$

$OH^\bullet + H^\bullet \rightarrow H_2O$

The suitable valence band edge potentials of both WO_3 and Ag_2O, i.e. +3.1 V and +1.39 V, respectively, are persuasive to split water with the generation of hydroxyl radicals. In the presence of methane in the system, a significant increase in H_2 production was observed for 1% and 5% Ag^+ loading (Fig. 8(a)), evidencing the increased $OH^\bullet$ radical generation compared to pure WO_3. The formation of additional H_2 in the presence of methane compared to water splitting for Ag^+ impregnated WO_3 can be regarded as an indicator for:

$$CH_4 + OH^\bullet \rightarrow CH_3OH + H^\bullet$$

$$CH_3OH + OH^\bullet \rightarrow CH_2OH \rightarrow CO_2 + H_2O$$

$$H^\bullet + H^\bullet \rightarrow H_2$$

$$OH^\bullet + OH^\bullet \rightarrow H_2O + {}^1\!/\!_2 O_2$$

$$OH^\bullet + H^\bullet \rightarrow H_2O$$

Scheme 3.

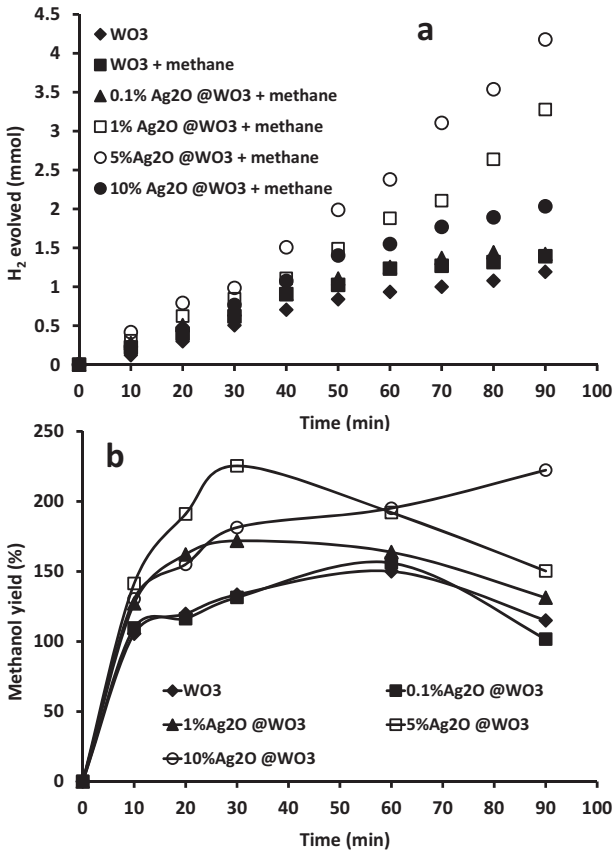

Fig. 8. (a) Comparison of H_2 generation over pure and Ag^+ impregnated WO_3 photocatalysts in the presence of methane. Methane was added to the catalyst suspension (300 mg/70 cm^3) at a flow rate of 100 ml/min for 15 mins. (b) Comparison of methanol yields over pure and Ag^+ impregnated WO_3 photocatalysts under laser illumination (100 mJ) in the aqueous medium. Methane was added to the catalyst suspension (300 mg/70 cm^3) at a flow rate of 100 ml/min for 15 mins.

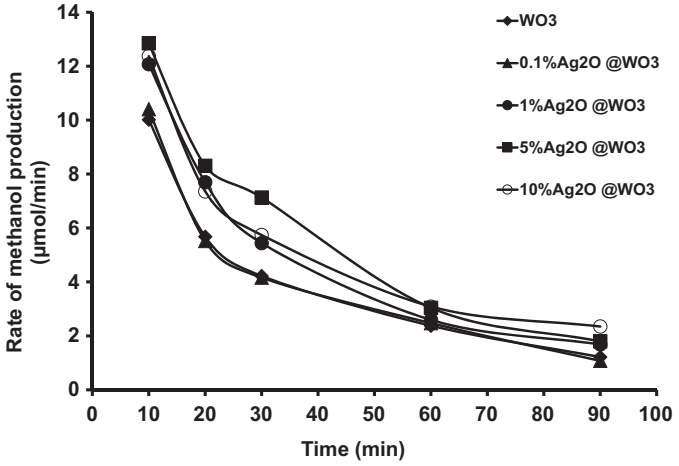

Fig. 9. Comparison of rate of methanol formation over pure and Ag^+ impregnated WO_3 photocatalysts (300 mg/70 cm^3) under laser illumination (100 mJ) in aqueous medium.

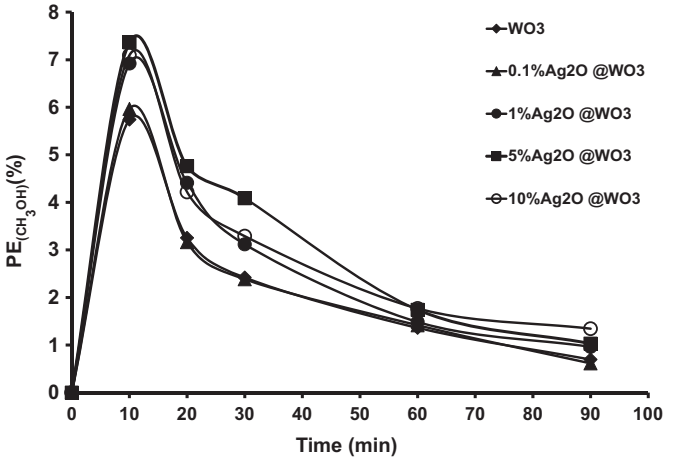

Fig. 10. Comparison of photonic efficiency (PE) over pure and Ag^+ impregnated WO_3 photocatalysts (300 mg/70 cm^3) under laser illumination (100 mJ) in aqueous medium.

(a) Extended lifetime of excited states.
(b) Increased ability of the impregnated catalysts for water oxidation.
(c) Interaction of $OH^•$ radicals (precursors for methanol) with methane molecules to displace $H^•$ radicals (precursors for H_2) in the bulk rather than at the surface of catalyst.

The comparison of methanol yields because of photocatalytic conversion of methane, over pure and Ag^+ impregnated WO_3 is presented in Fig. 8(b). A sharp initial increase followed by a rapid decrease was observed for pure WO_3, 1% and 5% Ag^+ impregnated catalysts. On the other hand, a gradually increasing trend for 10% Ag^+ loaded catalyst can also be observed. Methanol, a sacrificial molecule by nature, immediately after its formation competes with the water molecules for photogenerated holes results in its simultaneous degradation. Additionally the interaction of hydroxyl radicals with freshly formed methanol also results in a sharp decrease in methanol yield. The mineralization of methanol by superoxide radicals is not important, as the band edges of WO_3 are not suitable for the formation of superoxide radicals that requires a potential of −0.28 V. The decrease in the rate of formation of methanol as presented in Fig. 9, supports the same. A maximum yield of ∼47% (for a short span of time) was observed for 5% Ag^+ loading that was twice higher than pure WO_3. The gradual increase in methanol yield for 10% Ag^+ loading depicts that the photogenerated holes remain inaccessible to methanol molecules and the hydroxyl radicals are consumed either in methanol or oxygen formation. As mentioned in Scheme 3, the formation of $H^•$ radicals is mandatory in photocatalytic methane conversion process. Along with the formation of additional amounts of hydrogen, $OH^•$ radicals, owing to their non-selectivity, also initiate a number of side reactions leading to a variety of products that include acetone, acetic acid, acetaldehyde, di-methyl ether etc. Some of these products were identified during the analysis of samples but their concentrations were too low for quantification. All these free radical reactions also contribute in incrementing hydrogen yield.

The overall photonic efficiency (Fig. 10) of photocatalytic conversion process was found to be ∼8% which do not represent the actual photonic efficiency of process as it is impossible to account for all the processes occurring in the reaction. It only justifies the proportion of generated hydroxyl radicals, which interact with methane to form methanol in the fixed span of time. The remaining portion of photogenerated hydroxyl radicals is consumed in oxygen formation, interaction with methanol, interaction with methanol by-products such as formaldehyde etc. and recombination.

3.5.3. Photocatalytic degradation of methanol

The assumption of *in-situ* methanol degradation in photocatalytic conversion of methane into methanol was verified by performing the methanol degradation experiments. The methanol degradation profile of the catalysts used in the study is presented in Fig. 11, where it can be observed that the methanol degradation increases with the increase in Ag^+ loading. A maximum degradation of ∼45% was observed for 5% Ag^+ loading which again justifies the suppressed charge carrier recombination and increased production of hydroxyl radicals. As mentioned earlier, methanol can degrade either by competing with adsorbed H_2O molecules for donating electrons to h^+ or by direct interaction with $OH^•$ radicals as mentioned below in Scheme 4.

$$CH_3OH + h^+ \rightarrow CH_3OH^+ \rightarrow H_2CO + H^• + H^+$$

$$H_2CO + h^+ \rightarrow CO + H^• + H^+$$

$$CH_3OH + OH^• \rightarrow CH_2O + H^• + H_2O$$

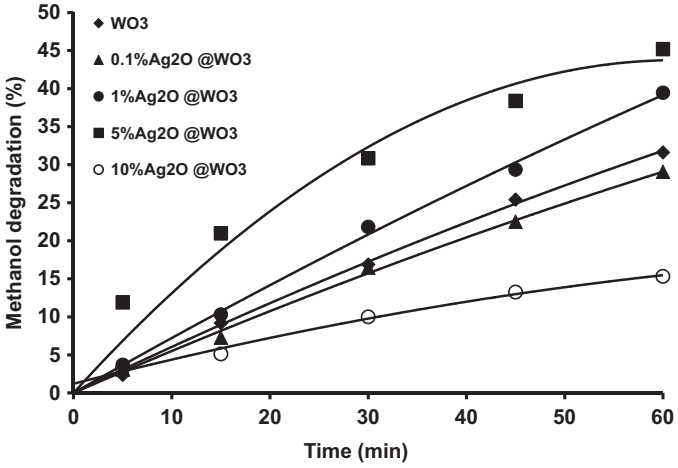

Fig. 11. Comparison of methanol degradation (percentage) over pure and Ag^+ impregnated WO_3 photocatalysts (300 mg/70 cm^3) under laser (355 nm, 100 mJ) illumination in aqueous medium containing 10 μL of methanol.

$$CH_3OH + h^+ \rightarrow CH_3OH^+ \rightarrow H_2CO + H^\bullet + H^+$$

$$H_2CO + h^+ \rightarrow CO + H^\bullet + H^+$$

$$CH_3OH + OH^\bullet \rightarrow CH_2O + H^\bullet + H_2O$$

Scheme 4.

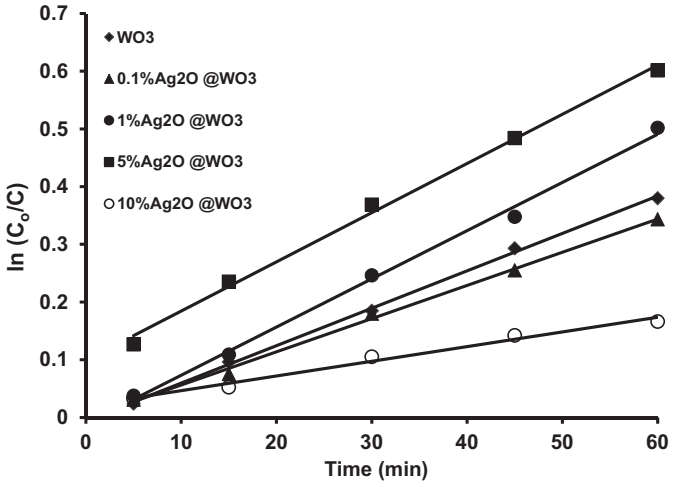

Fig. 12. Plot of $\ln(C_o/C)$ versus time for methanol degradation over pure and Ag^+ impregnated WO_3 photocatalysts (300 mg/70 cm^3) under laser (355 nm, 100 mJ) illumination in aqueous medium containing 10 μL of methanol.

For 10% Ag^+ loading the extent of methanol degradation was even lower than pure WO_3 verifying the assumption that 10% Ag^+ loading is sufficient enough to cover the whole surface of WO_3 thus behaving as independent catalyst. Secondly, the energy associated with 355 nm photons is sufficiently high enough to split up Ag_2O (1.2 eV) to form Ag^o. The kinetics of methanol degradation was evaluated by plotting $\ln(C_o/C)$ versus time as presented in Fig. 12, where it can be observed that photocatalytic degradation of methanol follows the pseudo first order kinetics.

4. Conclusions

The study has proved the practical viability of aqueous phase photocatalysis for the conversion of chemically/energetically inert molecules such as methane to useful oxygen containing compounds. However, the non-selectivity of photogenerated hydroxyl radicals initiates a variety of complex side reactions and electron-donating behavior of the product molecules limits the yield and selectivity of desired product. The study also revealed that methanol formation occurs through free radical mechanism originated after the diffusion of photogenerated hydroxyl radicals to the bulk. The study also establishes that the prerequisite for a photocatalyst to work as conversion catalyst is the suitability of valence band edge for splitting water with high efficiency. Although suitable for H_2 formation, photocatalyst with negative conduction band edge may have detrimental effect on the product yield by *in-situ* generation of oxidizing species like superoxide radicals. The presence of Ag^+ at the surface of WO_3 enhances the formation of hydroxyl radicals by suppressing the charge carrier recombination process however, the metal loading higher than 5% significantly affect the splitting/conversion process as photons are consumed in the dissociation of Ag_2O rather than being productive. The yield of methanol can be enhanced by continuous removal of the methanol after its formation. The study provides a base for the use of photocatalysis for synthetic purposes however much effort is still needed to optimize the process for higher yield.

References

[1] M.N. Chong, B. Jin, C.W.K. Chow, C. Saint, Water Res. 44 (2010) 2997–3027.
[2] T. Pradeep, Anshup, Thin Solid Films 517 (2009) 6441–6478.
[3] S. Malato, P. Fernandez-Ibanez, M.I. Maldonado, J. Blanco, W. Gernjak, Catal. Today 147 (2009) 1–59.
[4] N. Zhang, Y. Zhang, Yi-J. Xu, Nanoscale 4 (2012) 5792–5813.
[5] N. Zhang, Y. Zhang, Yi-J. Xu, Nanoscale 4 (2012) 2227–2238.
[6] E.J. Dlugokencky, K.A. Masarie, P.M. Lang, P.P. Tans, Nature 393 (1998) 447–450.
[7] R.H. Crabtree, Aspects of methane chemistry, Chem. Rev. 95 (1995) 987–1007.
[8] UNCED, U.N. Conference on Environment and Development UNCED "Earth Summit", Rio de Janeiro, Brazil, 1992.
[9] UNCED, U.N. Conference on Climate Change, UNCED Convention, Kyoto, Japan, 1997.
[10] UNCED, U.N. Conference on Global Warming and Environment, UNCED, Bonn, Germany, 2001.
[11] F. Sastre, V. Fornés, A. Corma, H. García, J. Am. Chem. Soc. 133 (2011) 17257–17261.
[12] P. Maruthamuthu, M. Ashokkomar, K. Gurunathan, E. Subramanian, M.V.C. Shastri, Int. J. Hydrogen Energy 14 (1989) 525–528.
[13] K. Ogura, M. Kataoka, J. Mol. Catal. 43 (1988) 371–379.
[14] P. Maruthamuthu, M. Ashokkomar, Int. J. Hydrogen Energy 14 (1989) 275–277.
[15] R.P. Noceti, C.E. Taylor, J.R. D'Este, US Patent 5720858, 1998.
[16] R.P. Noceti, C.E. Taylor, J.R. D'Este, Catal. Today 33 (1997) 199–204.
[17] C.E. Taylor, R.P. Noceti, Catal. Today 55 (2000) 259–267.
[18] C.E. Taylor, Catal. Today 84 (2003) 9–15.
[19] C.T. Brigden, S. Poulston, M.V. Twigg, A.P. Walker, A.J.J. Wilkins, Appl. Catal. B 32 (2001) 63–71.
[20] C.-F. Lien, M.-T. Chen, Y.-F. Lin, J.-L. Lin, J. Chin, Chem. Soc. (Taipei, Taiwan) 51 (2004) 37–42.
[21] V. Krishna, V.S. Kamble, P. Selvam, N.M. Gupta, Catal. Lett. 98 (2004) 113–116.
[22] T.M. Twesme, D.T. Tompkins, M.A. Anderson, T.W. Root, Appl. Catal. B 64 (2006) 153–160.
[23] K. Shimura, S. Kato, T. Yoshida, H. Itoh, T. Hattori, H. Yoshida, J. Phys. Chem. C 114 (2010) 3493–3503.
[24] K. Shimura, H. Yoshida, Energy Environ. Sci. 3 (2010) 615–617.
[25] I.R. Bellobono, F. Morazzoni, R. Bianchi, E.S. Mangone, R. Stanescu, C. Costache, P.M. Tozzi, Int. J. Photoenergy 7 (2005) 79–85.
[26] M.A. Gondal, A. Hameed, A. Suwaiyan, Appl. Catal. A 243 (2003) 165–174.
[27] M.A. Gondal, A. Hameed, Z.H. Yamani, A. Arfaj, Chem. Phys. Lett. 392 (2004) 372–377.
[28] J. Haber, J.H. Block, B. Delmon, Pure Appl. Chem. 67 (1995) 1257–1306.
[29] M.A. Gondal, A. Hameed, Z.H. Yamani, A. Suwaiyan, Chem. Phys. Lett. 385 (2004) 111–115.
[30] W. Dong, C. Zhu, J. Phys. Chem. Solids 64 (2003) 265–271.
[31] A.D. Yoffe, Adv. Phys 42 (2) (1993) 173–195.
[32] W.T. Dong, S.X. Wu, D.P. Chen, X.W. Jiang, C.S. Zhu, Chem. Lett. 5 (2000) 496–497.
[33] E. Sumesh, M.S. Bootharaju, A.T. Pradeep, J. Hazard. Mater. 189 (2011) 450–457.
[34] Y. Lai, H. Zhang, K. Xie, D. Gong, Y. Tang, L. Sun, C. Lin, Z. Chen, New J. Chem. 34 (2010) 1335–1340.
[35] J. Morales, L. Sánchez, F. Martin, J.R. Ramos-Barrado, M. Sánchez, J. Electrochem. Soc. 151 (2004) A151–A157.
[36] S.W. Gaarenstroom, N. Winograd, J. Chem. Phys. 67 (8) (1977) 3500–3506.
[37] J.F. Moulder, W.F. Stickle, P.E. Sobol, Handbook of X-ray Photoelectron Spectroscopy, Physical Electronics Inc, MN, USA, 1995.
[38] J. Zhang, J.P. Tu, X.H. Xia, Y. Qiao, Y. Lu, Sol. Energy Mater. Sol. Cells 93 (2009) 1840–1845.
[39] B.A. Deangelis, M. Schiavello, J. Solid State Chem. 21 (1977) 67–72.
[40] S.C. Moulzolf, S.A. Ding, R.J. Lad, Sens. Actuators, B 77 (2001) 375–382.
[41] G. Wang, Y. Ling, H. Wang, X. Yang, C. Wang, J.Z. Zhanga, Y. Li, Energy Environ. Sci. 5 (2012) 6180–6187.
[42] C. Cantalini, H.T. Faccio, M. Pelino, Sens. Actuators B 31 (1996) 81–86.
[43] B.V.R. Chowdari, P.P. Kumari, J. Mater. Sci. 33 (1998) 3591–3599.
[44] Y. Xu, M.A.A. Schoonen, Am. Mineral. 85 (2000) 543–556.
[45] W. Hou, B. Cronin, Adv. Funct. Mater. 23 (2013) 1612–1619.